DØ Note 4001

# First look at backgrounds to the search for the Higgs boson in the $\mathbf{H \to WW^{(*)} \to e\nu e\nu}$ channel in DØ data from Run 2

The DØ Collaboration
http://www-d0.fnal.gov/

**Abstract**

First data collected by the DØ experiment in Run 2 of the upgraded Fermilab Tevatron Collider have been used to assess the background from standard–model processes in $e^+e^-$ final states acompanied by missing transverse energy $\not\!\!E_T$. These topologies are expected to contain contributions from Higgs–boson production, with subsequent decay into two real or virtual $W$ bosons. The data, corresponding to an integrated luminosity of 8.8 pb$^{-1}$, show good agreement with expectations from the standard model. Applying all selection criteria, leaves one event, which is consistent with the expectation of 0.3±1.2 events. The low integrated luminosity does not as yet provide a significant constraint on the existence of a standard or a fermiophobic Higgs boson.

## 1 Introduction

The present note describes a study to assess the background in final states containing an $e^+e^-$ pair and missing transverse momentum in data collected by the DØ experiment at the Fermilab Tevatron Collider. The production of a standard model (SM) Higgs boson ($H$) is expected to contribute to this topology via the decay mode $H \to WW^{(*)} \to e\nu\ e\nu$. For SM decay, the cross section multiplied by the branching ratio is largest for

masses near $M_H = 160$ GeV/c$^2$. However, since it is only of the order of a few fb, the present data, corresponding to an integrated luminosity of 8.8 pb$^{-1}$, have no sensitivity to a standard–model Higgs boson.

Event rates are expected to be larger in alternative models, where either the production cross section or the branching fraction into $W$ pairs is enhanced. Such scenarios are realized, for example, in a fourth–generation model, where the Higgs production cross section is about a factor of 8.5 larger in the mass range 100 GeV/c$^2$ $< M_H <$ 200 GeV/c$^2$ [1]. In Fig. 1a, the enhancement factor for a fourth–generation model is shown as a function of the mass of the Higgs boson. The enhancement factor depend on the Higgs mass and on the masses of the quarks of the hypothetical fourth generation. In fermiophobic (or bosonic) Higgs models the coupling to fermions is suppressed leading to larger branching ratios for $W$ or $\gamma$ pairs [2]. The branching ratios for one of these models are presented in Fig. 1b as a function of the Higgs–boson mass.

The cross sections multiplied by branching ratios $\sigma\times$ B(H $\rightarrow$ WW$^{(*)}$ $\rightarrow$ e$\nu$e$\nu$) for the standard–model Higgs are given in Table 1, assuming the usual three generations, as well as an additional fourth generation of particles. The QCD–corrected results are taken into account at NLO for the gluon fusion process [3]. The enhancement factor from the fourth generation changes slightly for $M_H <$ 300 GeV/c$^2$, but is assumed to be $\approx$ 8.5 for the range under consideration. This specific value corresponds to a Higgs boson of $M_H = 160$ GeV/c$^2$, and a mass of $m_4 = 320$ GeV/c$^2$ for the fourth generation quarks. The current mass limit for a fourth generation is $m_4 >$ 199 GeV/c$^2$ [4].

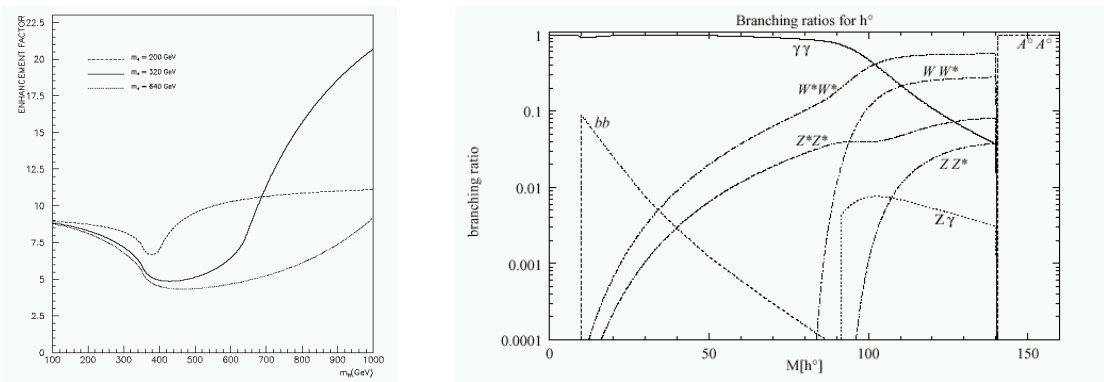


Figure 1: a) Enhancement factor for the Higgs boson production from gluon fusion via loops due to a fourth family of quarks [1] and b) branching fractions in a fermiophobic Higgs model [2].

$Z$ and virtual $\gamma^* \rightarrow$ee production represent the largest background processes for events with two electrons in the final state. These events can be separated from any possible Higgs–boson signal by exploiting the missing–transverse–energy $\not{E}_T$ signature. The pair production of vector bosons $WW, W\gamma$ and $ZZ$, with leptonic $W$ and $Z$ decays, represents an additional source of background events. Also $t\bar{t}$ production leads to

| $M_H$(GeV) | | 110 | 120 | 130 | 140 | 150 | 160 | 170 | 180 | 190 |
|---|---|---|---|---|---|---|---|---|---|---|
| $\sigma\times$B (fb) | SM | 0.45 | 1.06 | 1.82 | 2.46 | 2.81 | 3.05 | 2.71 | 2.18 | 1.52 |
| | $4^{th}$ Gen | 3.8 | 9.0 | 15.5 | 20.9 | 23.9 | 25.9 | 23.0 | 18.5 | 12.9 |

Table 1: $\sigma\times$ BR for the Higgs boson in the channel $H \to WW^{(*)} \to e\nu e\nu$ in the mass range 110 GeV/c$^2$ < $M_H$ < 190 GeV/c$^2$. The calculations are given for the standard model Higgs and for the model with a fourth generation. The cross sections for the standard model are taken from [5] and are multiplied by a factor of 8.5 to obtain the model with a fourth generation.

final states with two leptons, which are, however, accompanied by additional jets. Contributions can also arise from $W + jet$ and multi–jet production, where one or two jets are misidentified as leptons.

The data sample, and issues pertaining to trigger efficiency, luminosity and the basic electron identification criteria are discussed in Section 2 of this note. Section 3 presents additional selections for enhancing any signal from the Higgs boson. The Monte Carlo samples used to estimate expectations from background processes are presented in Section 4, which is followed in Section 5 by a detailed comparison between data and Monte–Carlo expectations for signal and background.

# 2 The Data sample

The data used in the present analysis were collected by the DØ experiment between February and June 2002. For the final state of interest, the di–electron stream of the DØ top–working group [6] provides an unbiased preselection, and has therefore been used in this study. In addition, only runs considered as *good runs* by the Jet/MEt group [7] have been retained for analysis.

Before presenting the analysis, we will first address the question of trigger bias and determination of luminosity.

## 2.1 Trigger and Trigger efficiency

Event selection is based on the *single–electron trigger* (EM_HI), which at Level 1 requires one electromagnetic (EM) trigger tower with $p_T > 10$ GeV/c (termed CEM(1,10)). In the data–taking period under consideration, this trigger was limited to the central region of the detector $|\eta_{det}| < 0.8$. The turn–on for Level 1 is shown in Fig. 2a. The trigger efficiency for electrons with $p_T > 20$ GeV/c (see Section 2.3), is greater than 95% [8]. At Level 3, the EM_HI filter requires one EM L3 object with EMFraction EMF > 0.9 and $E_T > 15$ GeV. The Level 3 turn–on for the central calorimeter is presented

in Fig. 2b. The efficiency obtained from data at Level 3 relative to Level 1 is essentially 100% for EM objects with $p_T > 20$ GeV/c. The trigger rates at Level 1 are 25 Hz, and 3.25 Hz at Level 3, for a luminosity of $1 \times 10^{31}\text{cm}^{-2}\text{s}^{-1}$. For $2 \times 10^{31}\text{cm}^{-2}\text{s}^{-1}$, the rates increase to 50 Hz at Level 1 and to 6.5 Hz at Level 3. The recently increased acceptance of the Level 1 calorimeter trigger should improve the signal efficiency by about a factor of 1.3.

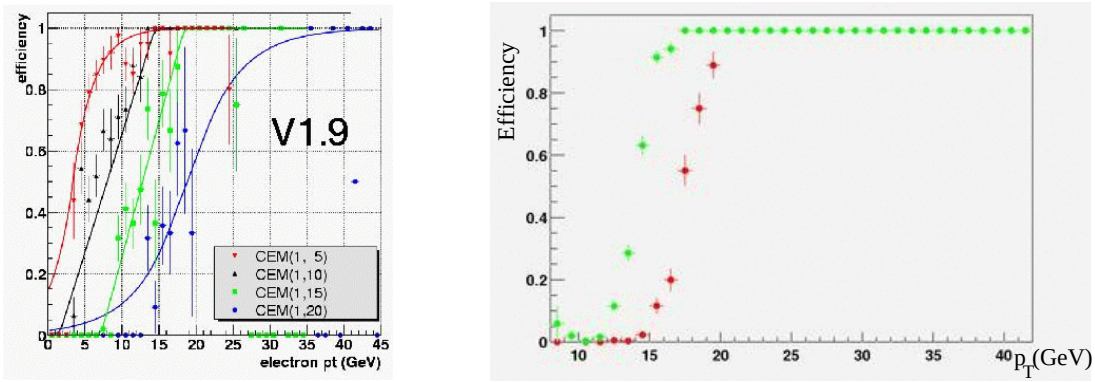


Figure 2: Turn–on for Level 1 for different single–electron triggers (left), and turn–on for Level 3 (right) for EM_HI.

## 2.2 Integrated luminosity

The integrated luminosity for the data sample considered was determined using two independent approaches, which are described in the following sections.

### 2.2.1 Integrated luminosity from luminosity blocks

For every trigger and reconstruction version of the standard DØ reconstuction program dØreco, the luminosity is recorded in luminosity blocks. During the data streaming process, the luminostiy block numbers are stored seperately in a histogram [6]. Using the lm_access package [9], the integrated luminosity can be calculated for every trigger. Events from only good luminosity blocks are used in the analysis, because it is not possible to normalize events from bad luminosity blocks. The integrated luminosities determined for the EM_HI trigger for different reconstruction versions are summarized in Table 2. The results are presented both with and without the *good run* selection requirements. The systematic uncertainty on the determined luminosity is ±10% [10].

| dØreco version | p10.15.00 | p10.15.01 | p10.15.02 | SUM |
|---|---|---|---|---|
| good luminosity blocks | 0.99 $pb^{-1}$ | 5.29 $pb^{-1}$ | 0.84 $pb^{-1}$ | 7.12 $pb^{-1}$ |
| + good run selection | 0.88 $pb^{-1}$ | 4.79 $pb^{-1}$ | 0.62 $pb^{-1}$ | 6.29 $pb^{-1}$ |

Table 2: Integrated luminosity for the EM_HI trigger and different versions of the reconstruction program. The integrated luminosities are listed without (top) and with (bottom) good run selection.

### 2.2.2 Integrated luminosity using $Z \to ee$ events

A greater fraction of the collected data can be retrieved if reliance on good luminosity blocks can be ignored. To use data with bad luminosity blocks, requires that the luminosity for those blocks be calculated from the ratio in the number of $Z \to ee$ events observed in the two data samples.

We implement this approach using the di–electron events reconstructed with version p10.15.01 of dØreco are used. The standard electron identification and kinematic criteria (see Section 2.3) are applied, but track matching is not required. The latter provides more data, and avoids additional uncertainties in the luminosity from uncertainties in the performance of the tracker. The di–electron mass distribution for events with good luminosity blocks is shown in Fig. 3. The observed mass spectrum can be described by a Gaussian signal and a background that can be parametrized by a polynomial. The $Z$-signal is determined by subtracting the fitted background from the data. To get the integrated luminosity for the whole sample, including bad luminosity blocks, the number of $Z \to ee$ events observed in this subsample has to be compared with the $Z \to ee$ events in the complete sample. The same procedure is used to estimate the number of $Z \to ee$ events in this second sample. Consequently, the integrated luminosity is given by

$$\int \mathcal{L}dt_{tot} \;=\; \int \mathcal{L}dt_{good} \cdot \frac{N_{tot}(Z \to ee) \text{ in the whole sample}}{N_{good}(Z \to ee) \text{ in good luminosity blocks}} \;. \qquad (1)$$

With $N_{good} = 253$ events, $N_{tot} = 463$ events and $\int \mathcal{L}dt_{good} = (4.79 \pm 0.48)$ $pb^{-1}$, the integrated luminosity for the complete sample is found to be $\int \mathcal{L}dt_{tot} = (8.8 \pm 1.1)$ $pb^{-1}$, and all results quoted in the following sections, both for signal and background, are based on this luminosity.

Using the $\gamma^*/Z$ Monte Carlo, it is possible to compare the number of expected and observed events. To calculate the number expected, the efficiency $\eta$ for the $Z$ Monte Carlo is determined after subtracting the Drell–Yan contribution the same way as done in the data. The product of the acceptance and trigger and reconstruction efficiencies

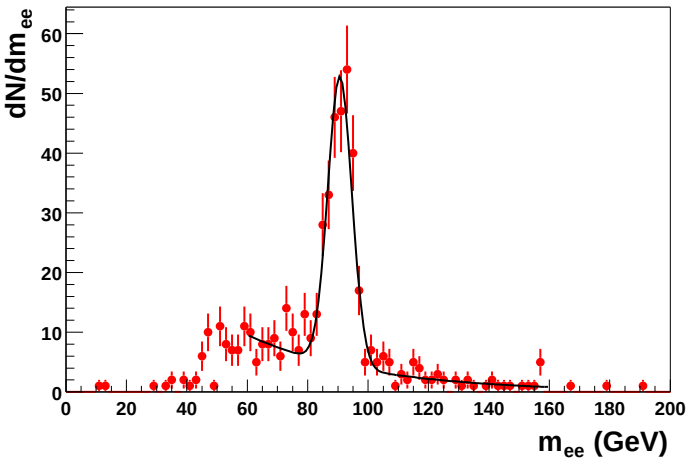


Figure 3: Distribution in di–electron mass ($m_{ee}$) for data with good luminosity blocks.

is determined from the fraction of events accepted in the $Z$–mass range

$$\eta = \frac{\text{reconstructed events}(80\ \text{GeV/c}^2 < m_{ee} < 100\ \text{GeV/c}^2)}{\text{generated events}(80\ \text{GeV/c}^2 < m_{ee} < 100\ \text{GeV/c}^2)} \tag{2}$$

From this result, and the measured cross section multiplied by the branching fraction $\sigma \times B(Z \to ee)$, the number of expected $Z$ events ($N_{pred}$) can be computed as follows:

$$N_{pred} = \int \mathcal{L}dt \cdot \sigma \times BR \cdot \eta \tag{3}$$

With $\int \mathcal{L}dt = 8.8$ pb$^{-1}$, $\eta = 0.246$ and $\sigma \times B(Z \to ee) = 218$ pb [11], the expected number of $Z$ events is $N_{pred} = 472$, which is in excellent agreement with the $N_{obs} = 463$ events observed in the data.

## 2.3 Electron Identification

The offline selections in the di-electron stream requires two reconstructed EM objects, with $p_T > 15$ GeV/c and $p_T > 12$ GeV/c for the first and second object, respectively. The events were reconstructed with versions p10.15.00, p10.15.01 and p10.15.02 of dØreco, and the corrections for calorimeter non–linearity and geometry (version 1.9) are applied to both EM clusters [8].

Starting from this initial selection of two EM clusters, corresponding to a total of 121,119 events, the event selection proceeds by imposing the following requirements:

- Presence of a single electron trigger bit for EM_HI, with a $p_T$ requirement of 10 GeV/c at Level 1

- Standard electron–identification criteria (isolation, EMFraction and HMatrix ) for the EM clusters. In addition, both EM clusters are to be in the fiducial region of the calorimeter, i.e $|\eta_{det}| < 1.1$ (CC) and $1.5 < |\eta_{det}| < 2.5$ (EC), with electron–identification parameters:

$$\begin{aligned} ISO &< 0.15 \\ EMF &> 0.90 \\ HMx8 &< 20.0\ . \end{aligned} \tag{4}$$

For the above criteria, the electron identification efficiency is observed to be 89.2% for electrons in the central calorimeter, and 95.1% for electrons in the end calorimeters [8]. Subsequently, the following criteria are applied to further improve background rejection:

- At least one of the EM clusters is required to have a track from the central tracker extrapolated to the psosition of the shower. (At the moment, such track matching can be implemented only in the central region, where the track–matching efficiency is found to be 65% [8]). The requirements for a track match are implemented through a combination of a $\chi^2$ (computed from E over p and $\Delta\phi$) and the distance of closest approach (DCA).

- To reduce the background from multi–jet production, and to minimize trigger bias, both electrons must have $p_T > 20$ GeV/c$^2$.

These selections provide 452 events, for which the $p_T$ spectrum of the leading lepton and the invariant mass of the electron pair ($m_{ee}$) are shown in Fig. 4.

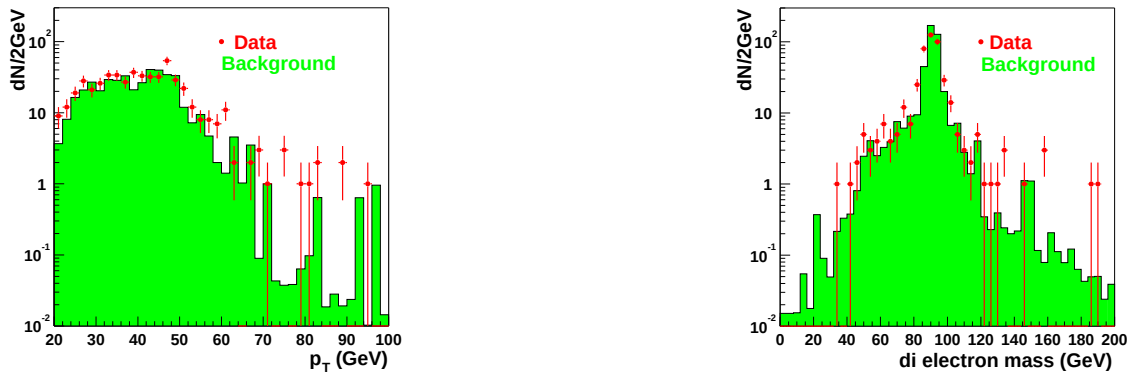


Figure 4: Distribution in leading–$p_T$ (left) and $m_{ee}$ (right) for data (crosses) and the sum of all backgrounds (filled histograms) (see Section 4).

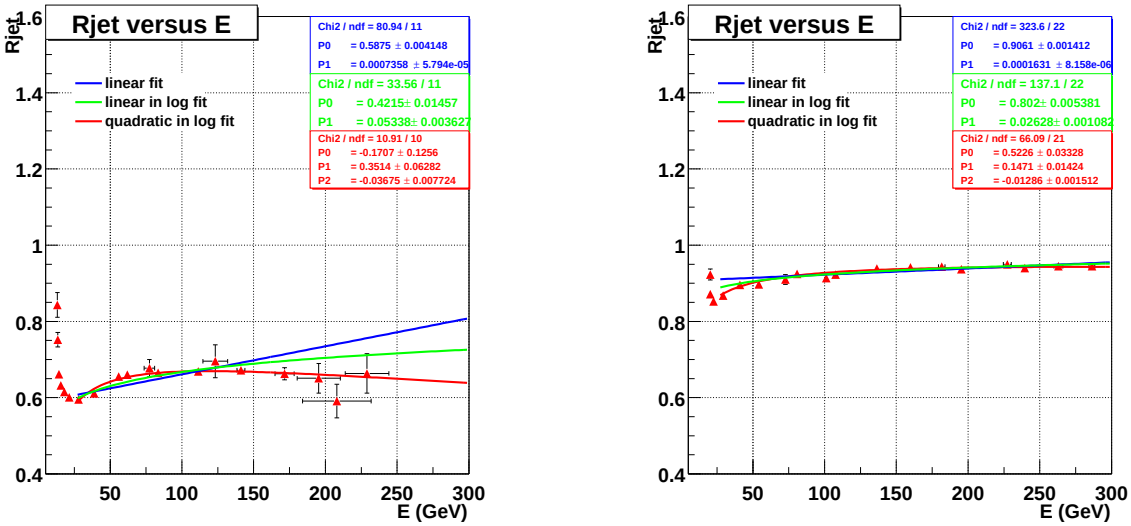


Figure 5: Calorimeter response as a function of jet energy for data (left) and plate Monte Carlo (right).

## 2.4 Jet energy scale

Energy corrections are applied to correct the calorimeter response to hadronic jets. This includes corrections for the spread of the shower outside of the the defining jet cone. This is done using the routine *JetCorr* version 2.1 [12]. Different corrections factors are applied for data, and for plate or mixture Monte Carlo. The factors for the cone algorithm with cone size R = 0.5 in Run 2 are shown as a function of jet energy in Fig. 5a for data, and Fig. 5b for plate Monte Carlo.

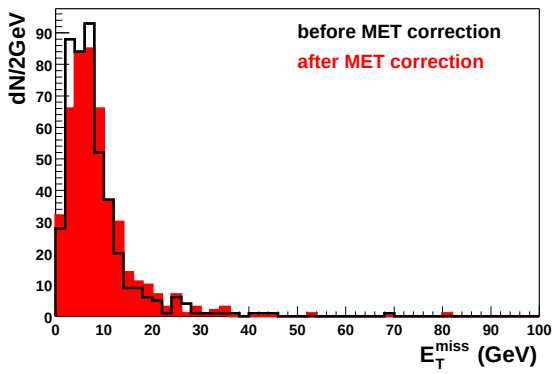


Figure 6: Missing transverse energy before (open histogrm) and after (filled histogram) application of jet energy corrections.

Clearly the missing transverse energy is affected by the jet corrections. Although the jets used in this analysis are reconstructed using R = 0.5 cones, the missing transverse energy is calculated using a jet cone size of R = 0.7. This is because the larger cone size provides an improved estimate of the missing energy correction. The vectorial changes in $E_T$ of the R = 0.7 cone jets are then vectorially to the original missing transverse energy and define the final missing transverse energy. The $\not\!\!E_T$ for data before and after correction is shown in Fig. 6.

# 3 Selection of signal

Production of Higgs bosons with their subsequent decay $\mathrm{H} \to \mathrm{WW}^{(*)} \to \mathrm{e}\nu\mathrm{e}\nu$ has characteristic features that can be exploited to enhance signal relative to background. One of these features is the anti-correlation of the $W$ spins from the decay of the scalar Higgs [13]. Because the $W^+$ and the $W^-$ have opposite spin projections, the charged lepton and antilepton tend to be emitted along the same direction, and are therefore expected to have small azimuthal separation $\Delta\phi_{\ell\ell}$, as well as small separation $\Delta R_{\ell\ell}$ in $\eta - \phi$ space. Since in the rest frame of the Higgs boson the $e^+e^-$ system and the $\nu\bar{\nu}$ system are emitted back to back with essentially equal energy, the invariant mass of the charged leptons, $m_{ee}$, is limited to $\sim \mathrm{M_H}/2$.

After the implementation of the above–described electron identification and kinematic criteria, the dominant background in the selected sample is from $Z \to ee$ decays. The distribution of the di-electron invariant mass $m_{ee}$ for the 452 selected events is shown in Fig. 4a. The peak from the $Z$ is clearly visible. To reject this contribution, a cut of $m_{ee} < 78$ GeV/c$^2$ is required. The distributions in $m_{ee}$ for signal ($M_H = 160$ GeV/c$^2$) and for different backgrounds are shown in Fig. 7. As can be seen, nearly all backgrounds are reduced substantially as a result of the requirement on $m_{ee}$, without having significant impact on signal. The acceptance is $\approx 93\%$ for a Higgs mass of 160 GeV/c$^2$.

No significant $\not\!\!E_T$ is expected for the background from multi–jet production or from di-electron events from $\gamma^*/Z$ contributions to the sample. Consequently, requiring

$$\not\!\!E_T \ > 20 \text{ GeV} \tag{5}$$

would be expected to improve the signal to background ratio. The $\not\!\!E_T$ distributions for signal with $\mathrm{M_H} = 160$ GeV/c$^2$ and for different backgrounds are shown in Fig. 8. Again, the $\not\!\!E_T$ requirement maintains high efficiency for signal, and rejects much of the multi–jet and $e^+e^-$ background. Events are also rejected when the missing transverse momentum vector points along the direction of any reconstructed jet. An R = 0.5 cone algorithm is used to reconstruct the jets. Requiring

$$\Delta\varphi(\not\!\!E_T, jets) \ > \ 0.5 \ , \tag{6}$$

rejects events where missing transverse momentum is caused by a mismeasurement of jet energy in the detector. Figure 9 presents the distribution in $\not\!\!E_T$ for data and backgrounds after applying the $m_{ee}$ criteria.

Background from additional jets in the final state, in particular for $t\bar{t}$ or $W$ + jet events, can be rejected by a veto on jets. All reconstructed jets with $p_T > 20$ GeV/c and $|\eta| < 2.5$, that are not associated with a reconstructed electron, are considered for event rejection. To distinguish additional jets from those associated with electron showers, it is required that $\Delta R$ between jets and electromagnetic clusters be $> 0.7$. The distributions in the number of these additional jets are shown in Fig. 10 for the Higgs

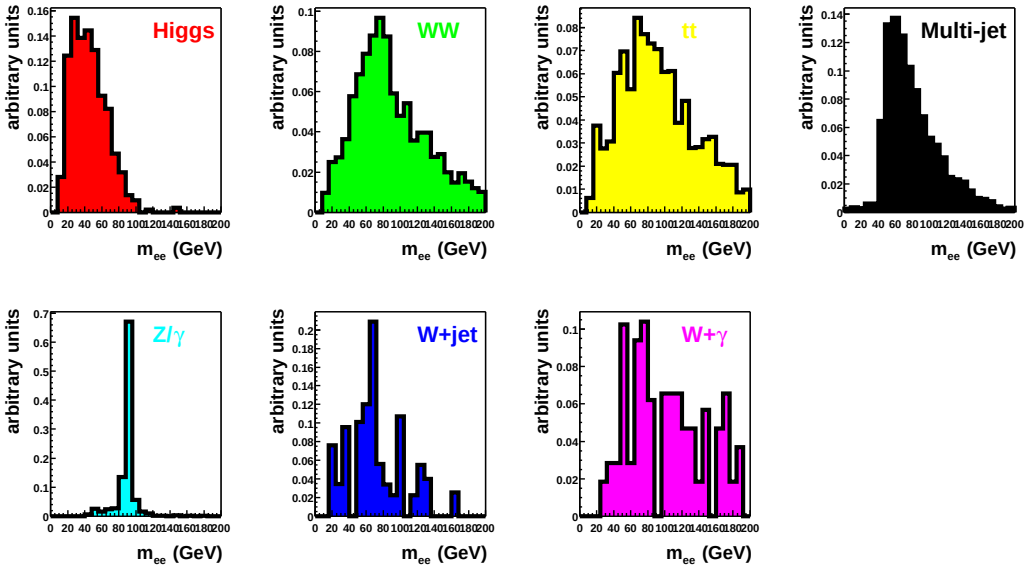


Figure 7: Distributions in di–electron mass $m_{ee}$ for Higgs signal for $\mathrm{M_H} = 160$ GeV/c$^2$, and for backgrounds from $WW$, $t\bar{t}$, multi–jet, $Z/\gamma$, $W$+jet and $W + \gamma$ production, after electron selection and implementation of the $p_T$ requirement.

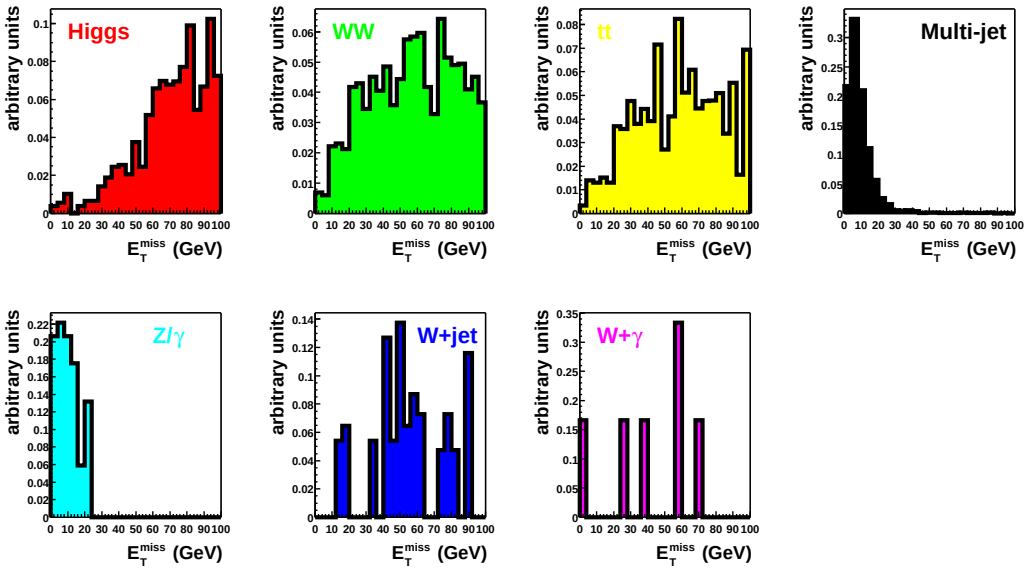


Figure 8: Distributions in $\not{E}_T$ for Higgs signal for $\mathrm{M_H} = 160$ GeV/c$^2$, and for backgrounds from $WW$, $t\bar{t}$, multi–jet, $Z/\gamma$, $W$+jet and $W + \gamma$ production, after electron selection, and the imposition of $p_T$ and $m_{ee}$ requirements.

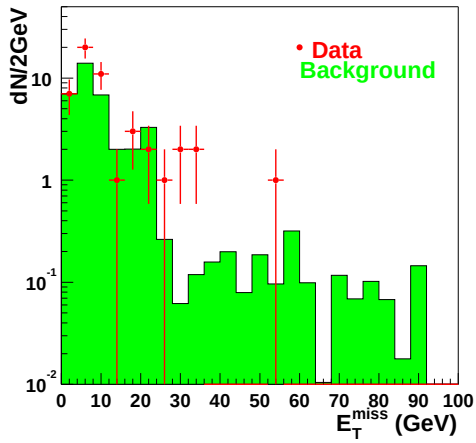


Figure 9: Distribution in $\not\!\!E_T$ for data (crosses) and the sum of all backgrounds (filled histogram) after the $m_{ee}$ criteria is applied.

signal and for background. At present, it is required that any eccepted event have no additional jet with $p_T > 20$ GeV/c. This restriction may be dropped in the future because it also affects the efficiency for Higgs (found to be only 75%). As discussed above, the opening angle for leptons from Higgs decays is expected to be small, which is not the case for many backgrounds, where leptons are expected to be emitted back to back, e.g., multi–jet or $\gamma^*/Z$ production. Requiring

$$\Delta\Phi_{ee} \quad < \quad 2.0 \ , \tag{7}$$

reduces the background without affecting signal.

The number of events remaining after the successive application of all selections is given in Table 3.

The selections reduce the data sample from 452 to one event. The largest reduction is from the restriction on $m_{ee}$, which suppresses the large contribution from $Z$ events.

| | DATA |
|---|---|
| ID, $p_T$>20GeV | 452 |
| + $m_{ee}$ <78GeV | 46 |
| + $\not\!\!E_T$ >20GeV | 5 |
| + jet veto | 2 |
| + $\Delta\Phi_{ee}$ <2.0 | 1 |

Table 3: Number of observed events after successive application of the indicated selections.

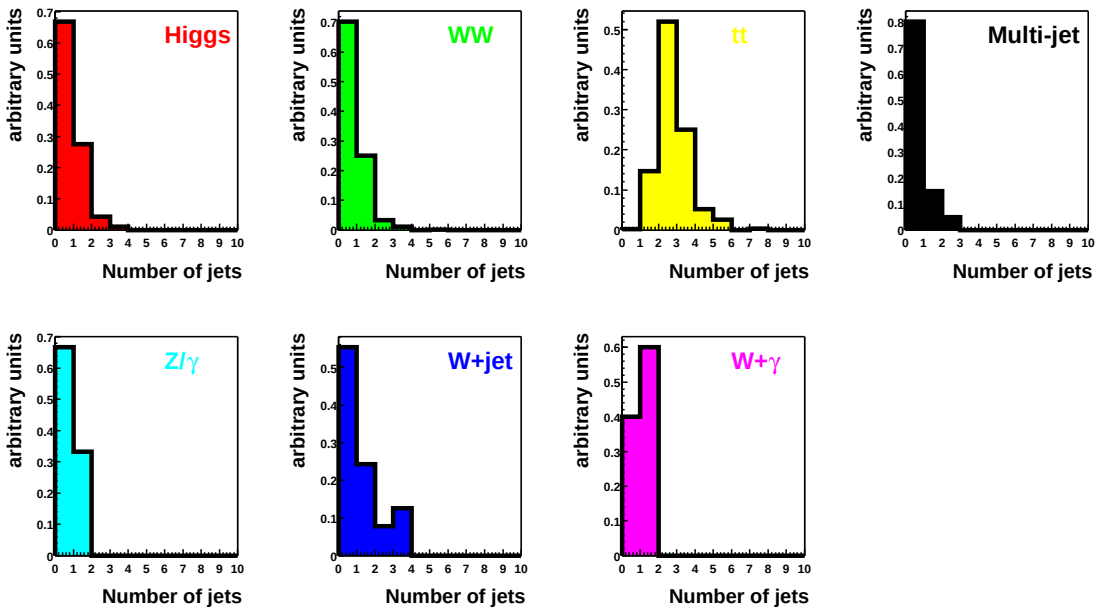


Figure 10: Number of reconstructed jets with $p_T > 20$ GeV/c that are not associated with electromagnetic clusters for the Higgs signal (for $\mathrm{M_H} = 160$ GeV/c$^2$) and for $WW$, $t\bar{t}$, multi–jet, $Z/\gamma$, $W$+jet and $W+\gamma$ backgrounds. The distributions are shown after electron identification and application of $p_T$, $m_{ee}$ and $\not{E}_T$ selection criteria.

Five events remain requiring $\not{E}_T > 20$ GeV, the $\not{E}_T$ and $\Delta\Phi_{ee}$ distributions for which are shown in Fig. 11. After applying the jet veto and the $\Delta\Phi_{ee}$ selection, only one event remains (dashed event in Fig.11). A display of this event is given in Fig.12.

# 4 Monte Carlo samples for signal and background

## 4.1 Signal Efficiencies

The signal efficiencies for the criteria described above were determined for a 160 GeV/c$^2$ mass value of a standard–model Higgs boson. The results are given in Table 4.

Because of the fiducial cut, which already reject 50% of the signal, and the relatively high $p_T$ requirement of 20 GeV/c for the electrons the signal acceptance starts at a level of 16% for the high–mass point. This is reduced to about 9% after all selections. This leads to an expectation of 0.02 signal events in the model involving a fourth generation. A looser $p_T$ requirement for the second electron of 15 GeV/c would gain a factor of 1.3 in signal efficiency.

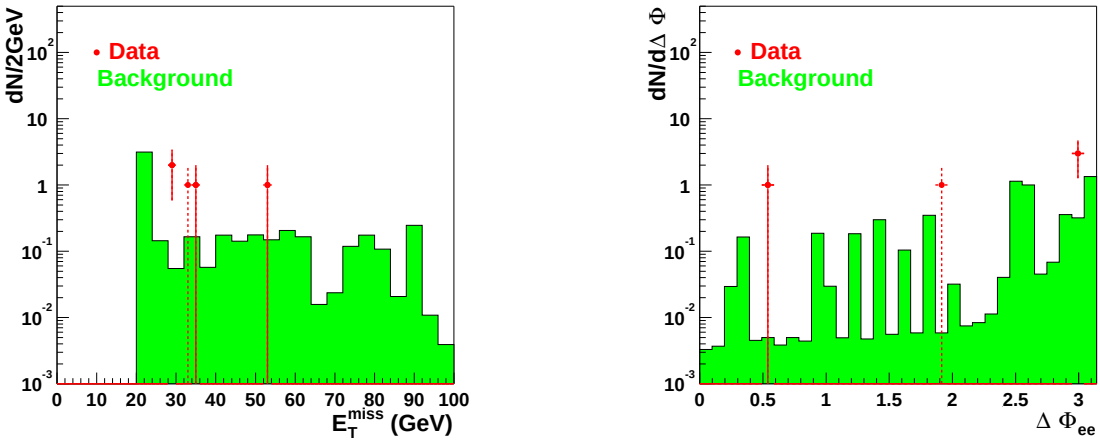


Figure 11: Distribution in $\not\!\!E_T$ (left) and $\Delta\Phi_{ee}$ (right) for the five remaining events, and for expected backgrounds, after $m_{ee}$ and $\not\!\!E_T$ selection.

| | Higgs efficiency (%) |
|---|---|
| $M_H$ (GeV/c$^2$) | 160 |
| ID, $p_T$>20GeV | 16.1±0.8 |
| + m(ll)<78GeV | 14.9±0.7 |
| + $\not\!\!E_T$ >20GeV | 13.1±0.7 |
| + jet veto | 9.8±0.6 |
| + $\Delta\Phi_{ee}$ <2.0 | 8.9±0.6 |

Table 4: Efficiencies for signal after electron identification and kinematic and other selections, for a Higgs boson with $M_H$ = 160 GeV/c$^2$.

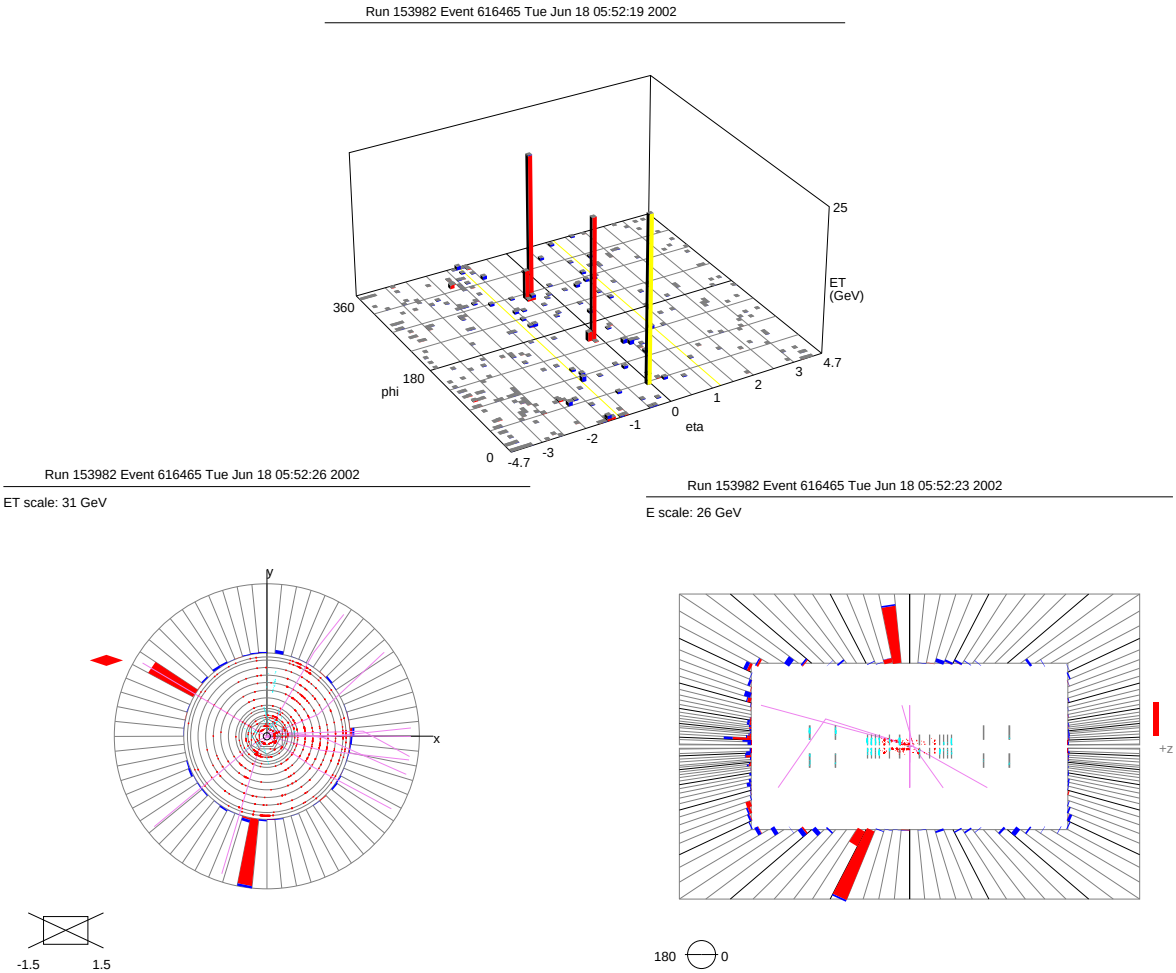


Figure 12: Lego plot in $\eta$ and $\phi$ and , (x,y) and (r,z) views for the remaining event. The transverse momenta of the two electrons are $p_T = 33.6$ GeV/c and $p_T = 26.4$ GeV/c, the di–electron invariant mass is $m_{ee} = 50$ GeV/c$^2$, the transverse missing energy is $\not{E}_T = 29.3$ GeV. This results in a transverse mass of $m_T = 118$ GeV/c$^2$.

## 4.2 Background processes with real electrons

All Monte Carlo samples (Higgs, $WW$, $t\bar{t}$, $Z/\gamma$, $W + jet$, $W+\gamma$) were generated with PYTHIA 6.155 [14], and processed through the full detector simulation and reconstruction chain. Except for the $W$+jet and $W+\gamma$ samples, the plate–geometry option was used in dØgstar. On average, 0.5 minimum–bias events were overlaid on these events. The reconstruction was done using dØreco p10.15.01, except for the $W + \gamma$ sample, which was reconstructed using version p10.11.00. The cross sections and the numbers of generated events are summarized in Table 5.

Except the $W + jet$ and multi–jet background, all other background samples have two genuine electromagnetic clusters. Photon clusters must also be considered in the background, since a track match is required for only one of the two electron candidates. Trigger efficiencies and efficiencies for calorimetric electron identification are taken from the Monte Carlo simulation. Due to DØ trigger restrictions for the reported data–taking period (see Section 2.1), one electron cluster is required to be in the central region of the detector $|\eta_{det}| < 0.8$.

To compare the reconstruction efficiency in data and Monte Carlo, the efficiency for plate Monte Carlo is computed using the $Z/\gamma^*$ sample. The reconstruction efficiency $\eta$ is obtained by comparing the number of events generated in the $Z$–peak ($N_{gen}$) with the number reconstructed within that peak ($N_{rec}$). Fiducial and $p_T$ criteria are applied at the generator (parton) level as well as on reconstructed events. Because of the trigger acceptance, one electron is required to be in the central calorimeter. With $N_{gen}$ = 394 and $N_{rec}$ = 324, the reconstruction efficiency is $\eta$ = 82.2%. To calculate the corresponding reconstruction efficiency from data, a distinction must be made between events with both electrons in the central calorimeter (33% of the Monte Carlo events) and those with one electron in the end calorimeters (67%). Taking this into account, the reconstruction efficiency for di–electron events from data is $(83.1 \pm 3.9)$%, which is

| | | $\sigma \times B$ [pb] | generated events |
|---|---|---|---|
| 1 | $\mathrm{H} \to \mathrm{WW}^{(*)} \to \mathrm{e}\nu\mathrm{e}\nu$ ($\mathrm{M_H}$ = 110 GeV/c$^2$) | 0.0018 | 2000 |
| 2 | $\mathrm{H} \to \mathrm{WW}^{(*)} \to \mathrm{e}\nu\mathrm{e}\nu$ ($\mathrm{M_H}$ = 160 GeV/c$^2$) | 0.0120 | 2000 |
| 3 | $WW \to e\nu e\nu$ | 0.094 | 25000 |
| 4 | $t\bar{t} \to e\nu be\nu\bar{b}$ | 0.074 | 4682 |
| 5 | $Z \to ee$ | 218 | 6250 |
| 6 | $W + jet \to e\nu + jet$ | 1164 | 25898 |
| 7 | $W + \gamma \to e\nu + \gamma$ | 4.75 | 1054 |

Table 5: $\sigma \times BR$ and number of generated events for the different Monte Carlo samples. The cross section for the channels (1) – (4) are taken from the Tevatron Higgs Working Group Report [5], for Channel (5) it is taken from Ref. [11], and for Channels (6) and (7) are obtained from studies with PYTHIA [14].

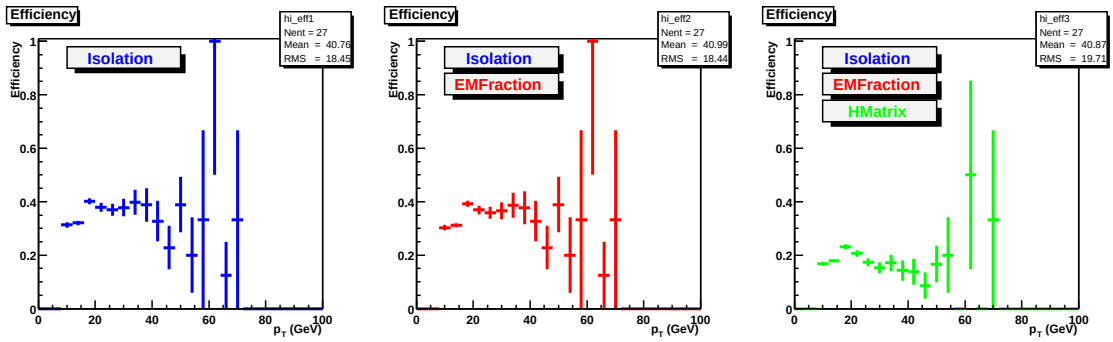


Figure 13: Acceptance factors for jets from multi–jet events after successive application of Isolation (left), EMFraction (middle) and HMatrix criteria (right).

in good agreement with the 82.2% found from Monte Carlo.

Because the current Monte–Carlo simulation does not reproduce the track–matching efficiency, no track–matching requirements are applied in the Monte Carlo. Instead, the efficiency of 65% is taken from data.

For $W + jet$ events, only one electron is present in the final state, and the second one arises from misidentification of an accompanying jet. Due to limited statistics of the $W$+jet Monte Carlo sample, it is not possible to evaluate this misidentification rate by applying electron–identification criteria to the second electron candidate. That is, after applying all identification and kinematic criteria, only a few events remain, and the statistical uncertainty on the estimated rate is very large. Consequently, these cutoffs are not imposed on the Monte Carlo, but rather the events are weighted to reduce these uncertainties. The rejection factors for electron–identification are determined using Monte Carlo simulation of multi–jet events that are generated as a function of transverse momentum ($p_T$ > 10 GeV/c, $p_T$ > 20 GeV/c, $p_T$ > 40 GeV/c and $p_T$ > 80 GeV/c). This is done because the current integrated luminosity gives insufficient statistical precision for determining the rejection factors directly from data. The results obtained from the Monte Carlo are shown in Fig. 13, where the successive rejection factors for the Isolation, for the EMFraction, and for the HMatrix criteria are shown as a function of the jet $p_T$.

## 4.3 Multi–jet background obtained from data

The background contribution from multi–jet production to the di-electron and $\not\!\!E_T$ final state was determined directly from DØ data. The di–electron stream is used again to obtain a sample of EM–like jets. All electron identification and $p_T$ selections are applied, as indicated before, but with the HMatrix criteria inverted for the EM

candidates. That is, requiring poor electrons, or

$$HMx8 \ > \ 20 \tag{8}$$

for both EM clusters. This reduces greatly the true electrons in the sample. The shape of the $\Delta\Phi_{ee}$ distribution for these events is parametrized using the form:

$$f \ = \ p_0 + p_1 \cdot exp(p_2 \cdot \Delta\Phi_{ee}). \tag{9}$$

The distribution in $\Delta\Phi_{ee}$ for the selected events is shown in Fig. 14a, together with the corresponding fit

$$f \ = \ 6.03 + 0.00067 \cdot exp(4.52 \cdot \Delta\Phi_{ee}) \ , \tag{10}$$

which describes the data quite well.

The effect of the selection criteria described in Section 2 were determined using this same multi–jet sample, and the results are listed in Table 6.

The final prediction for the background from multi–jet production is obtained as follows. First, the contributions from all processes, except for the multi–jet background, are subtracted from the search sample (with HMx8 $<$ 20). The multi–jet background is obtained by normalizing Eq. (10) to the remaining events in the region $\Delta\Phi_{ee} > 2.5$, where multi–jet production is dominant. This fit is extrapolated to the region of expected signal ($\Delta\Phi_{ee} < 2.0$), and determines the final contribution of the multi–jet background in the region of interest.

# 5 Comparison between data and expectations from Monte Carlo

As mentioned before, after implementation of the electron–identification and basic kinematic criteria, the data sample consists of 452 events. A large fraction of these events arise from $Z$-production, for which the Monte Carlo predicts 410$\pm$20 events. All other processes (with the exception of multi–jets) contribute less than 2 events.

| | Rejection factor |
|---|---|
| $m_{ee} < 78$ GeV/c$^2$ | 1.93 |
| + $\not\!\!E_T > 20$ GeV | 24.4 |
| + jet veto | 27.0 |

Table 6: Cumulative rejection factors for "electron" background from multi–jet production, after implementation of the initial electron–identification and kinematic criteria.

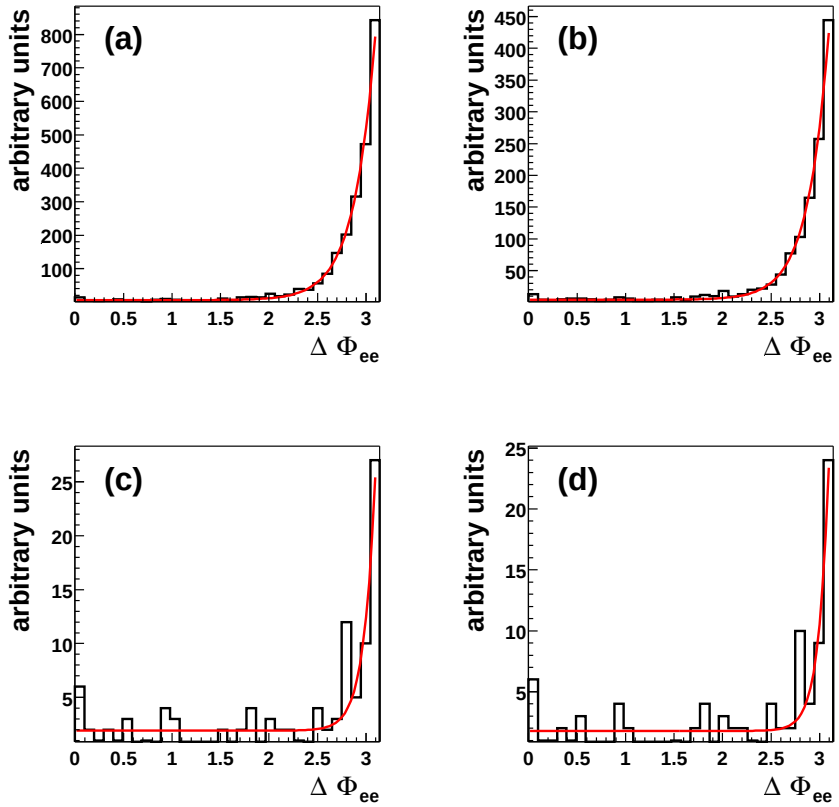


Figure 14: Distribution in $\Delta\Phi_{ee}$ for EM–like jet background from multi–jet production, overlayed with the fit to the shape of Eq. (10), after imposing electron and kinematic selections (a), and (b) after (a) and the $m_{ee}$ requirement, (c) after (b) and $\not{E}_T$ selection, and (d) after (c) and jet veto.

After normalization in the region of high $\Delta\Phi_{ee}$, the multi–jet background is found to be 18±4.5 events. Consequently, within statistical uncertainty, the total number of expected events is consistent with what is observed in the data.

The details of the contributions from different background sources are given in Table 7, where it can be observed that the sum of the background events at every stage of the analysis is in agreement with the number of observed events. After all selections are applied, only one event is left in the data sample, which agrees with the sum of all the background events of 0.3±1.2. The uncertainty is dominated by the limited statistics of the $\gamma^*/Z$ Monte Carlo. The distributions in $\Delta\Phi_{ee}$ for data and Monte Carlo, after the implementation of all criteria, are presented in Fig. 15.

From the acceptances and efficiencies, and an integrated luminosity of $\int \mathcal{L}dt = 8.8$ pb$^{-1}$, the predicted number of events for a Higgs boson with a mass of $\mathrm{M_H} = 160$

GeV/c$^2$ and an enhancement from a fourth generation of quarks, is 0.02 events. The distribution of a potential Higgs signal is shown in Fig. 15.

| | $WW$ | $t\bar{t}$ | QCD | $Z$ |
|---|---|---|---|---|
| ID, $p_T$>20GeV | 0.18±0.0012 | 0.10±0.0035 | 18±4.5 | 410±20 |
| + $m_{ll}$ <78GeV | 0.08±0.0008 | 0.05±0.0022 | 10±2.5 | 23±4.7 |
| + $\not\!\!E_T$ >20GeV | 0.06±0.0007 | 0.03±0.0019 | 0.8±0.2 | 2.8±1.5 |
| + jet veto | 0.05±0.0007 | $(0.1\pm0.03)\cdot10^{-3}$ | 0.7±0.2 | 1.9±1.3 |
| + $\Delta\Phi_{ee}$ <2.0 | 0.03±0.0006 | $(0.8\pm0.02)\cdot10^{-4}$ | 0.04±0.01 | 0±1.2 |

| | $W$+jets | $W+\gamma$ | Sum | DATA |
|---|---|---|---|---|
| ID, $p_T$>20GeV | 1.5±0.27 | 0.7±0.14 | 430±21±54 | 452 |
| + $m_{ll}$ <78GeV | 1.2±0.23 | 0.6±0.07 | 35±5±4 | 46 |
| + $\not\!\!E_T$ >20GeV | 0.8±0.21 | 0.2±0.06 | 4.9±1.2±0.6 | 5 |
| + jet veto | 0.3±0.18 | 0.1±0.05 | 3.1±1.2±0.4 | 2 |
| + $\Delta\Phi_{ee}$ <2.0 | 0.2±0.16 | 0.05±0.02 | 0.3±1.2±0.04 | 1 |

Table 7: Expected number of backgrounds events, and the number of events observed in the data, after application of successive selections for an integrated luminosity of $\int \mathcal{L}dt$ = 8.8 pb$^{-1}$. The statistical error is listed for all backgrounds, the systematic error due to the uncertainty on the luminosity is only given for the sum of all backgrounds.

# 6 Conclusion

A search has been performed for di-electron final states with missing transverse momentum in DØ data recorded in Run 2 since February 2002. The number of observed events is consistent with expectations from standard background processes at all stages of the analysis. Because of the small integrated luminosity, the data do not as yet have sensitivity to a standard–model Higgs boson, nor to alternative models involving a fourth generation of quarks. Improvements are expected in the near future from both an increase in integrated luminosity and from improved performance of the detector. In addition, the selection criteria will be optimized as a function of Higgs mass.

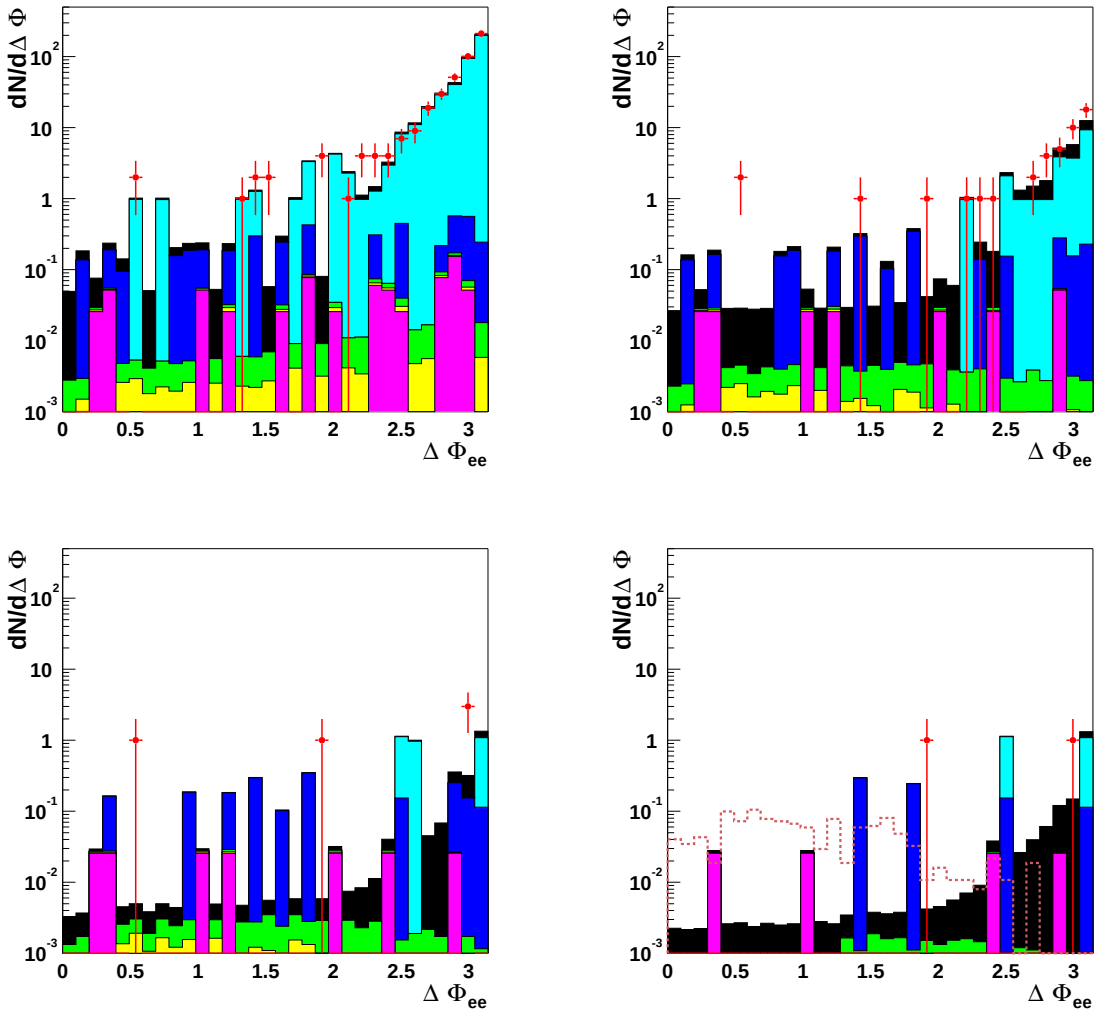


Figure 15: Distributions in $\Delta\Phi_{ee}$ for signal (crosses) and the background: multi–jet (black), $Z/\gamma$ (light blue), $W$+jet (dark blue), $WW$ (green), $t\bar{t}$ (yellow) and $W+\gamma$ (magenta). The distributions are shown after the initial electron–identification and kinematic selections (top left), and for successive application of $m_{ll} < 78$ GeV/c$^2$ (top right), $\not\!\!E_T > 20$ GeV (bottom left) and jet veto (bottom right). The shape of a possible Higgs signal ($\mathrm{M_H} = 160$ GeV/c$^2$), multiplied by a factor of 50, is overlaid (dashed line) in the last plot. All acceptances and efficiencies for signal have been taken into account.

# References


[1] E. Arik *et al*, SN–ATLAS–2001–006.

[2] L. Brücher, R. Santos, hep–ph/9907434.

[3] M. Spira, hep–ph/9801289.

[4] D. E. Groom *et al*, The European Physical Journal **C15**, (2000) 1.

[5] M. Carena *et al*, Report of the Tevatron Higgs Working Group, hep–ph/0010388.

[6] E. Barberis *et al*, DØ Note 3942.

[7] DØ Jet/MEt group, Good Run Selection 1.5.
`http://www-d0.fnal.gov/~d0upgrad/d0_private/software/jetid/certification/Macros/Runsel-after-Moriond/v1.5/runsel-1.5.html`

[8] DØ EM–ID group, EM–ID certification 1.9.
`http://www-d0.fnal.gov/phys_id/emid/d0_private/certification/main_v1_9.html`

[9] S. H. Ahn *et al*, DØ Notes 3971, 3972, 3973.

[10] R. Partridge, private communication.

[11] S. Abachi *et al*, Phys. Rev. Letters 75 1456 (1995).

[12] DØ Jet Energy Scale group, Jet Energy Scale v2.1.
`http://www-d0.fnal.gov/phys_id/jes/d0_private/tools/jetcorr.txt`

[13] M. Dittmar, H. Dreiner, Phys. Rev. D55, 167–172, (1997).

[14] T. Sjöstrand, Comp. Phys. Comm **82**, 74, (1994).